

## PRECISION LIMITS TO EMISSION-LINE PROFILE MEASURING EXPERIMENTS

J. IRELAND

L3Com Government Services, Inc., NASA Goddard Space Flight Center, Mail Code 682.3, Building 26, Room G-1,  
Greenbelt, MD 20771; ireland@cdso8.nascom.nasa.gov

Received 2004 March 26; accepted 2004 November 5

### ABSTRACT

Spectra, such as astrophysical spectra, can provide detailed diagnostics on the state of their emitting volume. Emission-line diagnostics are found by assuming a model for the spectral emission line and then fitting the model to the data. It is shown for Poisson noisy emission-line data, via the application of Cramér-Rao lower bounds, that there are limits to the precision that line fitting can achieve. The limits depend on the spectral line model and the noise properties of the data. A Cramér-Rao lower bound treatment introduces a framework in which questions of line fitting in particular and spectrometers in general may be posed. Some example applications are given and their implications for the design of spectrometric observations are discussed.

*Subject headings:* instrumentation: spectrographs — methods: analytical — methods: statistical —  
Sun: transition region — Sun: UV radiation

### 1. INTRODUCTION

Astrophysics, like many other sciences, makes extensive use of spectrometers to measure emission lines. By modeling common approaches to the problem of fitting an emission-line model to spectral data and using Cramér-Rao lower bound theory, a framework can be constructed in which questions concerning the *precision* limits of idealized experiments can be answered.

Consider an experiment in which multiple measurements of the same quantity are made. Each time the experiment is run, the value observed is a sample from the distribution of measurements possible. The experiment is said to be precise if a “large proportion” of the samples lie “close” to the sample mean. In addition, the experiment is said to be accurate if the sample mean is “close” to the true value (the meaning of “close” is deliberately vague, since this depends on the purpose of the experiment). This definition of precision does not imply that a precise experiment need be accurate, since the sample mean could be very far from the true value yet be very precisely measured. Systematic errors in the experiment setup are one reason why a precise experiment need not be accurate.

One way of measuring whether a large proportion of the samples are close to the sample mean is to calculate the standard deviation of the experiment; smaller standard deviations imply that the experiment is more precise. The standard deviation is an unbiased estimator of the square root of the true variance of the distribution from which the measurements are drawn. Cramér-Rao lower bound theory (Rao 1945; Cramér 1946; Kendall & Stuart 1973) describes lower limits to the true variance and so can be interpreted as describing precision limits to experiments (Barford 1985). Experimental accuracy is *not* commented on, being outside the scope of applicability of the Cramér-Rao formalism.

The Cramér-Rao lower bound approach allows one to include the spectrometer itself in consideration of the line-fitting problem, and thus an exploration of the applicability of Cramér-Rao lower bounds to line fitting is also an exploration into the effect the spectrometer itself has on the information we can derive. An example of this can be found in Winick (1986), in which a Cramér-Rao lower bound argument is used to find the optimum pixel size such that the precision with which the location of a Gaussian emission line is maximized. Larger pixel sizes allow more pho-

tons to be collected and so the signal-to-noise ratio in each pixel is smaller. However, smaller pixels allow the line position to be better determined because there are more pixels per unit wavelength. The payoff between these two competing demands results in an optimum pixel size. Related questions of interest can be answered using the combination of an emission model, a spectrometer model, and Cramér-Rao formalism.

Some previous work does exist concerning the errors in the Gaussian parameters when fitting a Gaussian to noisy data. Landman et al. (1982) discuss the error associated with fitting a Gaussian emission line under the simplifying assumptions that (1) the data consist of a single emission line, (2) all data associated with the line have the same Gaussian distribution, and (3) the pixel width is much smaller than the line width. Lenz & Ayres (1992) expand this treatment to cases in which the Gaussian profile is subject to different noise properties via a Monte Carlo approach, but do not include a theoretical treatment. The Cramér-Rao approach creates a theoretical framework of some useful generality.

### 2. FORMALISM

#### 2.1. Maximum Likelihood and the Cramér-Rao Lower Bound

A spectrometer observes an intensity emission profile  $\mathbf{D} = \{D_1, D_2, \dots, D_{N_d}\}$  over  $N_d$  channels at  $\mathbf{x} = \{x_1, x_2, \dots, x_{N_d}\}$ . The features in the spectra, such as emission lines, background emission, and artifacts, are described using a total of  $N_v$  variables, where  $N_v < N_d$ . Hence, fitting the observed spectrum with  $N_v < N_d$  variables becomes an optimization problem. The variables form a set  $\mathbf{V}$ , and describe the number of counts per channel through an appropriate choice of function  $F(\mathbf{x}, \mathbf{V}) \equiv F_i(\mathbf{V})$ . It is up to the observer to pick an  $F$  and  $\mathbf{V}$  that adequately describe the emission spectra for their particular purpose. For example, in solar applications the choice is complicated by the fact that many solar plasmas are inhomogeneous in density, temperature, ionic composition, etc. In addition, the plasma is temporally inhomogeneous over the integration time of the exposure and spatially inhomogeneous along the line of sight and across the field of view. The values found for the variables  $\mathbf{V}$  are almost inevitably weighted averages of the true range of values in the observed emitting volume. This paper does not address the relation of the

spectrum to the true physical state of the emitting volume. However, once the observer has chosen  $F(\mathbf{x}, \mathbf{V})$  the precision with which the variables  $\mathbf{V}$  can be determined is, as is shown below, calculable. Discussion of the particular choice of  $F$  and  $\mathbf{V}$  is deferred until § 3.

The variable set  $\mathbf{V}$  describes the spectrum observed. Multiple observations show that the data  $D_i$  in each channel is noisy, and since the spectrum is described by  $\mathbf{V}$ , the noise in each channel  $i$  can be described by some normalized probability distribution  $f_i(D_i|\mathbf{V})$ . Assuming that the distribution function in each channel is independent of every other distribution function, the overall probability distribution function is therefore

$$L(\mathbf{D}, \mathbf{V}) = f_1(D_1|\mathbf{V})f_2(D_2|\mathbf{V}) \dots f_{N_d}(D_{N_d}|\mathbf{V}). \quad (1)$$

The function  $L$  is known as the likelihood function (LF). The maximum likelihood principle directs us to choose the value of  $\mathbf{V}$ ,  $\mathbf{V}_0$ , such that for any admissible value of  $\hat{\mathbf{V}}$

$$L(\mathbf{D}, \mathbf{V}_0) \geq L(\mathbf{D}, \hat{\mathbf{V}}). \quad (2)$$

In practice it is common to use the log likelihood function to look for  $\mathbf{V} = (V_1, \dots, V_{N_v})$  such that

$$\frac{\partial \log L}{\partial V_j} = 0, 1 \leq j \leq N_v. \quad (3)$$

$\hat{\mathbf{V}}$  is a maximum of equation (1) if the matrix

$$\left[ \frac{\partial^2 \log L}{\partial V_p \partial V_q} \right]_{\hat{\mathbf{V}}} \quad (4)$$

is negative definite where  $1 \leq p, q \leq N_v$ .

Take  $t$  as an unbiased estimator of some function of  $\mathbf{V}$ , say  $\tau(\mathbf{V})$ . It can be shown that (Kendall & Stuart 1973)

$$\text{var}(t) \geq \sum_{p=1}^{N_v} \sum_{q=1}^{N_v} \frac{\partial \tau}{\partial V_p} \frac{\partial \tau}{\partial V_q} \mathbf{I}^{-1}, \quad (5)$$

where  $\mathbf{I}$  is the (Fisher) information matrix,

$$I_{pq} = E \left( \frac{\partial \log L}{\partial V_p} \frac{\partial \log L}{\partial V_q} \right) = -E \left( \frac{\partial^2 \log L}{\partial V_p \partial V_q} \right), \quad (6)$$

where  $E(\cdot)$  denotes the expectation value of the parenthetical quantity (evaluation at the global maximum  $\mathbf{V}_0$ ). Equation (5) is known as the Cramér-Rao inequality for a multivariate estimator. It expresses the fact that the variance  $\text{var}(t)$  of an unbiased estimator of the function  $\tau(\mathbf{V})$  is bounded below. If the function is set to one of the emission model variables, then the theorem says that any unbiased estimator used to estimate the value of the variable has a minimum attainable variance. This implies that there is a limit to the precision of an experiment measuring the variables  $\mathbf{V}$  via the emission model  $F(\mathbf{x}, \mathbf{V})$ . To evaluate equation (5), note that

$$\left[ \frac{\partial^2 \log L}{\partial V_p \partial V_q} \right]_{\mathbf{V}_0} = E \left( \frac{\partial^2 \log L}{\partial V_p \partial V_q} \right), \quad (7)$$

that is, the expected value of  $\partial^2 \log L / \partial V_p \partial V_q$  occurs at the global maximum of the likelihood function. This defines a formally simple procedure for finding precision limits to an experiment. One finds  $\mathbf{V}_0$  and then evaluates equation (5) using equation (7). Finding  $\mathbf{V}_0$  is a global optimization problem and is, in general, nontrivial, although good estimates may be found by common line-fitting routines. For demonstration purposes (§ 3),

however, test cases are used in which the value of  $\mathbf{V}_0$  is known, i.e., everything is known about the emission. The remaining pieces of the framework needed to describe spectrometer experiments in a Cramér-Rao formalism are described below.

## 2.2. Emission Model and Poisson Noise

Attention is restricted to noise arising from the statistical nature of the emission process from the emitting region. Other sources of measurement error (both statistical and systematic) are not considered, since one source of error is sufficient to demonstrate the applicability of the Cramér-Rao formalism. The emission in solar plasmas is assumed to follow Poisson statistics, and so if channel  $i$  measures  $D_i$  counts, then the distribution function  $f_i$  in each channel is

$$f_i(D_i|\mathbf{V}) = \frac{[F_i(\mathbf{V})]^{D_i}}{D_i!} \exp[-F_i(\mathbf{V})] \quad (8)$$

for some emission model  $F_i(\mathbf{V})$ . Subsequently,

$$\log L = \sum_{i=1}^{N_d} D_i \log [F_i(\mathbf{V})] - [F_i(\mathbf{V})] - \log(D_i!), \quad (9)$$

and so the  $p, q$ th element of the information matrix is

$$I_{pq} = \sum_{i=1}^{N_d} \frac{1}{F_i(\mathbf{V})} \frac{\partial F_i(\mathbf{V})}{\partial V_p} \frac{\partial F_i(\mathbf{V})}{\partial V_q}, \quad (10)$$

which is evaluated at  $\mathbf{V} = \mathbf{V}_0$ . The observer is interested in the value of emission model variables,  $V_k$  ( $1 \leq k \leq N_v$ ), and so  $\tau = V_k$ . Then any unbiased estimator  $t$  of  $V_k$  must have

$$\text{var}(t) \geq [\mathbf{I}^{-1}]_{kk}, \quad (11)$$

where the right-hand side of this equation is the Cramér-Rao lower bound to  $\text{var}(t)$ .

The emission model describes features in the spectrum. In solar physics, it is common to assume that the emission lines have a Gaussian shape and that the background emission has a quadratic dependence on wavelength (or its proxy, position on the detector  $\mathbf{x} = \{x_1, x_2, \dots, x_{N_d}\}$ ). Hence,

$$F_i(\mathbf{V}) = \mu + \nu x_i + \xi x_i^2 + \sum_{j=1}^{N_g} A_j \exp \left[ -\frac{(x_i - c_j)^2}{2\sigma_j^2} \right], \quad (12)$$

where  $\mathbf{V} = (\mu, \nu, \xi, A_1, c_1, \sigma_1, \dots, A_{N_g}, c_{N_g}, \sigma_{N_g})$  is the set of variables with which we describe the emission features in the spectrum. Values to the variables  $\mathbf{V}$  are found by fitting the model equation (12) to the data  $\mathbf{D}$ , for example, by the method of least squares.

The final component in the description of an experimental setup is to model how the spectrometer is operated. To do this, the operation of the Coronal Diagnostic Spectrometer (CDS; Harrison et al. 1995) on board the *Solar and Heliospheric Observatory (SOHO)* is taken as a template of spectrometer operation. CDS is an extreme-ultraviolet spectrometer covering wavelengths in the range 150–800 Å using two spectrometer systems. The Normal Incidence Spectrometer (NIS) has two gratings that disperse two wavelength ranges, 308–381 Å (NIS1) and 513–633 Å (NIS2) (the Grazing Incidence Spectrometer observes spectra in four wavelength ranges, 151–221, 256–338, 393–493, and 656–785 Å). Light is admitted to the NIS via a slit, and images are built up by rastering the slit across the target. In each NIS study the entire

wavelength range mentioned above is exposed to the CCD but only portions of the exposed CCD are stored because of memory requirements. This fixes a range to  $x$  and data  $D$ , which is modeled by equation (12). Example applications of the Cramér-Rao formalism are based on the Fe xvii  $\lambda 360.76$  emission observed by CDS in the execution of the SYNOP\_F (ver. 1) study. In this study, a window of emission from 360.123 to 361.386 Å is observed using 18 pixels and is modeled using a constant background emission ( $\mu = 114$  photons pixel<sup>-1</sup>) and a single Gaussian emission line ( $A = 1434$  photons pixel<sup>-1</sup>,  $\sigma = 1.62$  pixels) usually centered in the window ( $c = 0.0$  pixels, unless otherwise specified).

The applications below are *not* intended to model the precision behavior of CDS, but are intended to demonstrate the range of applicability of a Cramér-Rao approach to describing the precision aspects of general spectrometer experiments.

### 3. APPLICATION OF THE CRAMÉR-RAO LOWER BOUND

The formalism above allows one to examine the precision possible in a number of different scenarios. Section 3.1 demonstrates the dependence of the Cramér-Rao lower bound on the number of unknowns in the system. Sections 3.2, 3.3, and 3.4 look at the dependence of minimum variance on how the emission line is sampled. Section 3.5 examines the dependence of minimum variances on the signal-to-noise ratio, while § 3.6 compares the results of multiple fittings using different fitting routines to the Cramér-Rao lower bound. Finally, § 3.7 shows that a Cramér-Rao lower bound analysis can be used to design a spectrometer observation such that the standard deviation in the total integrated intensity is minimized, that is, the experiment is optimized to be as precise as possible.

#### 3.1. Number of Unknowns

The most fundamental parameter in the formalism is the number of unknowns in the model. This expresses what is certain and what is unknown and therefore to be experimentally determined. To illustrate this, a spectrum is modeled as a constant background plus one Gaussian, a special case of equation (12) with  $\mu$  as the only unknown to be determined by fitting. If  $F_i(V) = \mu + Ag_i$ , for  $g_i = \exp[-(x_i - c)^2/(2\sigma^2)]$ , then

$$I_{11} = \sum_{i=1}^{N_d} \frac{1}{\mu + Ag_i} \quad (13)$$

leads to

$$\min \text{var}(\mu) \equiv v_{\mu,1} = 1/I_{11} \geq \mu/N_d, \quad (14)$$

which is the minimum achievable variance in measuring the background in the presence of a known emission line is greater or equal to the variance expected from  $N_d$  measurements of a constant value  $\mu$  subject to Poisson statistics; it is clear that the greater noise due to the emission line causes this. Similarly, if the Gaussian amplitude is the only unknown, then

$$I_{22} = \sum_{i=1}^{N_d} \frac{g_i^2}{\mu + Ag_i} \quad (15)$$

and the Cramér-Rao lower bound is

$$\min \text{var}(A) \equiv v_{A,1} = 1/I_{22} \geq A/N_d, \quad (16)$$

where the right-hand side is the variance expected from  $N_d$  measurements of a constant value  $A$  subject to Poisson statistics. Consider now the effect of having both  $\mu$  and  $A$  unknown

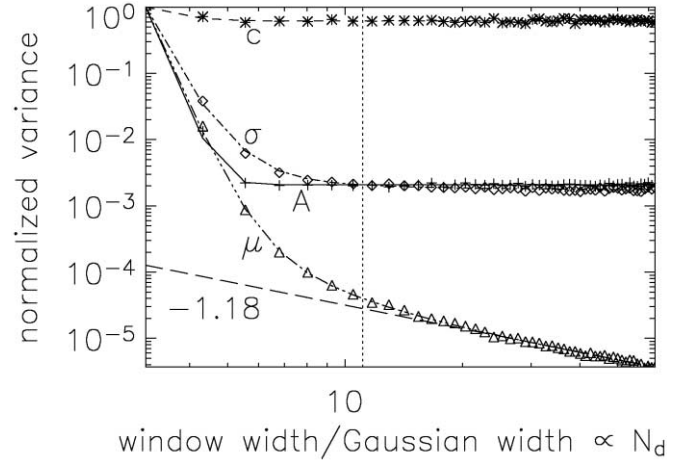


FIG. 1.—Precision as a function of window width (see § 3.2) for Fe xvii emission line (§ 2.2) properties (Gaussian amplitude  $A$ , solid line; line position  $c$ , dashed line; Gaussian width  $\sigma$ , dot-dashed line; constant background,  $\mu$ , triple-dot-dashed line). The vertical dotted line shows the size of the window used in CDS. Also shown is a power-law fit of the form  $N_d^\delta$  (long-dashed line) to the background variance, annotated with the value of the power-law index  $\delta$ . The plot symbols (Gaussian amplitude, plus signs; line position, asterisks; Gaussian width, diamonds; constant background, triangles) show variances derived from  $2^{10}$  spectrum fits at sample window widths.

in the emission model  $F_i(V) = \mu + Ag_i$ . The information matrix is  $2 \times 2$  in this case,

$$\mathbf{I} = \begin{bmatrix} I_{11} & I_{12} \\ I_{12} & I_{22} \end{bmatrix}, \quad (17)$$

where  $I_{12} = \sum_{i=1}^{N_d} g_i/(\mu + Ag_i)$ . Hence, we have

$$\min \text{var}(\mu) = \frac{I_{22}}{I_{11}I_{22} - I_{12}^2} \geq v_{\mu,1} \quad (18)$$

and

$$\min \text{var}(A) = \frac{I_{11}}{I_{11}I_{22} - I_{12}^2} \geq v_{A,1}. \quad (19)$$

The presence of another unknown increases the minimum variances attainable: the experiment has become less precise. For a nonzero Gaussian the experiment is strictly less precise than in the one variable unknown case.

#### 3.2. Increasing Window Size

The idealized spectrometer setup described in § 2.2 allows the user to return portions of the solar spectrum that illuminate the detector. A window width and location is defined, and the emission in that window is taken as the emission spectrum. Clearly, the width of this window ( $N_d$ ) affects the amount of information available on the emission line and therefore the achievable precision. The right-hand side of equation (11) is calculated for increasing values of  $N_d$  and plotted in Figure 1; also plotted are the variances derived from the results of fitting  $2^{10}$  simulated emission spectra at different window widths. Statistical fluctuations aside, the simulation-derived values follow the theoretically predicted behavior.

The emission-line amplitude, width, and position precisions quickly asymptote to fixed values as a function of window size. The background emission, however, continues to decrease as a function of window width, varying approximately as  $1/N_d$ . The difference in behavior between the background and the other

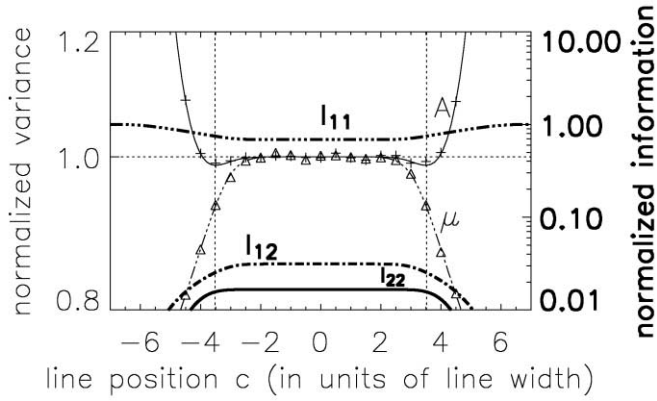


FIG. 2.—Normalized Cramér-Rao lower bound for Gaussian amplitude  $A$  (solid line) and background  $\mu$  (dashed line) as a function of line position in a spectral window of fixed size. The plot symbols (amplitude, plus signs; background, triangles) show variances derived from  $2^{18}$  spectrum fits at each line position (normalized to values at  $c = 0$ ). Bold lines show arbitrarily normalized information matrix elements (eq. [17]:  $I_{11}$ , associated with background emission;  $I_{22}$ , associated with the Gaussian amplitude; and  $I_{12}$ , a background and amplitude cross term). The vertical dotted lines denote the positions of minima in the Cramér-Rao lower bound for Gaussian amplitude.

variables is because increasing the window width increases the amount of information we get on the background much faster than the other variables. The simpler case outlined in equation (17) illustrates this; the ratios of summands in the definition of equation (17) are

$$\text{summand}(I_{22})/\text{summand}(I_{11}) = g_i^2$$

and

$$\text{summand}(I_{12})/\text{summand}(I_{11}) = g_i.$$

Having assumed above that the line is centered in the window, increasing  $N_d$  steps farther from the emission peak, where there are fewer photons due to the line and more due to background. In this situation,  $I_{11}$  increases linearly with  $N_d$ , whereas the other quantities in the matrix will tend to constants. On inversion, the Cramér-Rao lower bound for the background decreases linearly with  $N_d$ , whereas the others decrease much more slowly and are effectively constant.

An analysis of experimental precision as a function of window width allows one to design studies so that the window is not overly large, which (depending on the instrument) could save on processor time, onboard storage, and telemetry. The purpose of the observation and the instrument design must all be taken into account when optimizing a particular observation.

### 3.3. Location of the Line in the Spectral Window

The information content of the emission spectrum is also changed by the location of the line in the spectral window. CDS studies attempt to put the emission line of interest at the center of the window and so obtain the largest number of photons associated with the emission line. The Cramér-Rao formalism can be used to calculate precisions as a function of line location in the window, whether due to Doppler shift or deliberately not having the line centered in the window (moving the line center is equivalent to moving the window location).

An illustrative case of the influence of line position in the window is shown in Figure 2. It is assumed that both the line position and line width are known, leaving only the emission-

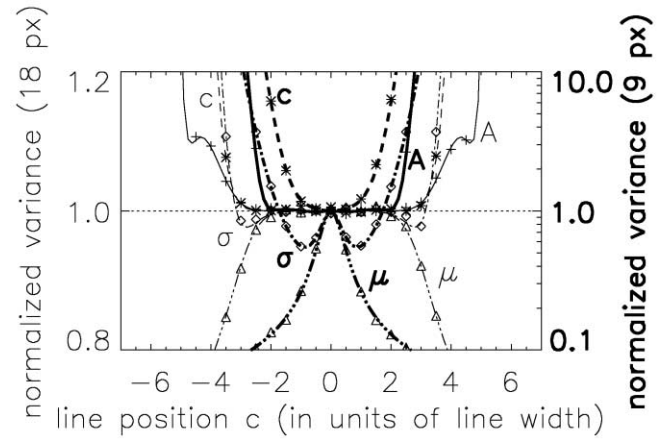


FIG. 3.—Normalized Cramér-Rao lower bounds for three Gaussian variables (amplitude, solid line; position, dashed line; width, dot-dashed line) and a constant background (triple-dot-dashed line) for window sizes of 18 and 9 pixels (bold lines). Plot symbols (Gaussian amplitude, plus signs; line position, asterisks; Gaussian width, diamonds; constant background, triangles) show normalized variances derived from  $2^{18}$  spectrum fits at each line position. All data are normalized to Cramér-Rao lower bound values at  $c = 0$ .

line amplitude and background emission unknown, that is, equations (18) and (19) as a function of line center  $c$ . Precisions in background get better as the line moves away from the center (as expected), since the window contains more and more background than emission line. Precisions in amplitude are best at  $c = \pm 3.52$  ( $\sim 2\%$  better) and not at  $c = 0$ , where the line is centered in the window. Intuitively, one would expect that the precision for Gaussian amplitude would get worse as the line moves out of the window. However, in the system as a whole, while it is true that the amount of information about the Gaussian amplitude decreases as the line moves out of the window, it is also true that the amount of information about the background emission increases. There comes a point when the decrease in amplitude information is more than compensated by the increase in information from the background; the final interdependence of this information is expressed in the Cramér-Rao lower bound through the inversion of the information matrix (the dependence as a function of line center of the different elements  $I_{11}$ ,  $I_{12}$ ,  $I_{22}$  of the information matrix  $I$  are shown in Fig. 2). The interplay of information also occurs in more complicated situations: Figure 3 compares the Cramér-Rao lower bound and variances derived via simulation for a Fe xvii line moving across the spectral window when all four variables in the simulation (three Gaussian variables and a constant background) are unknown.

When Fe xvii  $\lambda 360.76$  is observed on the Sun, the Doppler velocities measured rarely exceed  $\pm 150 \text{ km s}^{-1}$ , or  $\sim \pm 1.5$  line widths, implying that the spectrometer setup of § 2.2 will not experience gross changes in Cramér-Rao lower bound in typical observing circumstances. However, this need not always be the case. Reducing the number of pixels across the line to  $N_d = 9$  (Fig. 3) shows the effect of having less information. Cramér-Rao lower bounds for the constant background, line width, and position are more strongly affected in the region  $-1.5 \leq c \leq 1.5$  line widths. The structure seen in the Cramér-Rao lower bounds reflects the interplay of different amounts of information on each variable affecting the final bound. Such a study demonstrates that not only the amount of information but where that information comes from with respect to the emission feature being measured and the spectral window used can affect precisions.

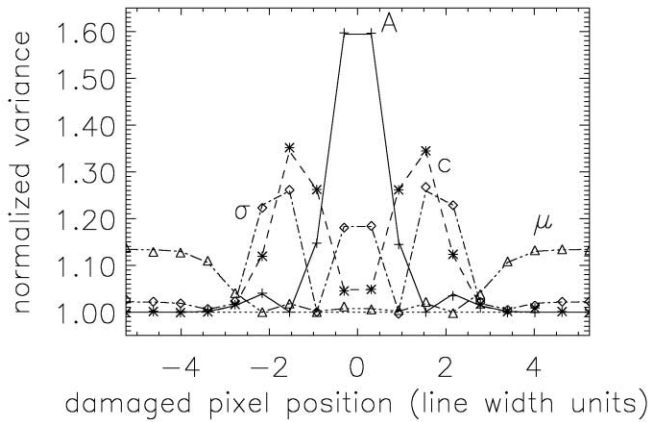


FIG. 4.—Normalized Cramér-Rao lower bounds (Gaussian amplitude, *solid line*; line position, *dashed line*; Gaussian width, *dot-dashed line*; constant background, *triple-dot-dashed line*) as a function of the damaged pixel position. Plot symbols (Gaussian amplitude, *plus signs*; line position, *asterisks*; Gaussian width, *diamonds*; constant background, *triangles*) show variances derived from  $2^{18}$  spectrum fits at each line position. All data are normalized to Cramér-Rao lower bound values calculated when all 18 pixels are included in the calculation.

### 3.4. Damaged Detector Pixel

Figure 4 demonstrates the effect on precisions of having a single damaged pixel (say, due to cosmic ray or charged particle hits) in an observation of the Fe xvii line (§ 2.2) as a function of the position of the damaged pixel. The damaged pixel is assumed to contribute no information to the information matrix  $I$ . The resulting Cramér-Rao lower bounds are all larger relative to the full information case, as expected. The degree to which each quantity is affected depends on the location of the damaged pixel; for example, the experiment becomes much less precise in measuring the Gaussian amplitude when the damaged pixel is within one line width of the emission center than when the damaged pixel lies greater than two line widths away from the line center. The converse is true for the background, reflecting the relative importance of these locations to each variable expressed, as through the inverse of the information matrix. Such a study may be useful in redesigning experiments to optimize goals when confronted with a damaged spectrometer. For example, consider a spectrometer experiment in which the pixels close to line center are damaged. If photon counting is a primary goal and is judged to be more important than deriving Doppler velocities, a combination of the studies outlined here and in § 3.3 could be used to judge how best to reimagine the line to obtain better precision in Gaussian amplitude.

### 3.5. Influence of Line-to-Continuum Ratio

A simple way to increase the number of photons per pixel is to increase the exposure time used. Let  $\zeta \geq 1$  be the ratio of the new (longer) exposure time to the previous exposure time. The number of photons collected can be modeled as  $\zeta F_i(V)$ , which implies  $\text{var}(t) \geq [I^{-1}]_{kk}/\zeta$  (eq. [11]). The Cramér-Rao lower bounds in all variables vary as  $1/\zeta$ , or inversely with exposure time, implying that precision increases linearly with exposure time.

Consider instead an experiment in which the background number of counts stays the same but the number of counts in the emission line changes. This could occur, for example, if a change in the experiment design changes its stray light characteristics. Such an effect can be modeled through  $\beta A/\mu$ , for  $\beta \geq 0$ . This varies the line-to-continuum ratio and its effect is shown in

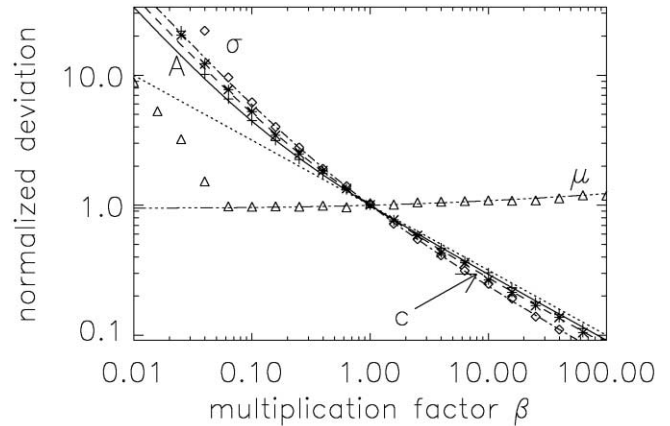


FIG. 5.—Normalized deviation lower bounds of each variable (Gaussian amplitude  $A$ , *solid line*; Gaussian position  $c$ , *dashed line*; Gaussian width  $\sigma$ , *dot-dashed line*, and background  $\mu$ , *triple-dot-dashed line*) as a function of  $\beta$  (see § 3.5). The plot symbols (Gaussian amplitude, *plus signs*; line position, *asterisks*; Gaussian width, *diamonds*; constant background, *triangles*) show deviations derived from  $2^{10}$  spectrum fits at sample values of  $\beta$ . These data are normalized to the deviation values at  $\beta = 1$  and the variable values. Also shown (*dotted line*) is the line  $\beta^{-1/2}$ .

Figure 5. Plotted here are normalized deviations, calculated via the square root of the variance, divided by the variable value (except Gaussian position).

The behavior of the normalized deviations can be understood through looking at the Cramér-Rao information matrix components. For the Gaussian amplitude, the leading term is  $I_{11}$ . As  $\beta \rightarrow \infty$ ,  $I_{11} \propto \beta$ , and so the normalized deviation varies as  $\beta^{-1/2}$ . The leading term for the Gaussian position in the information matrix can be found by considering equation (10) for  $V_p = c$ , that is,

$$I_{33} = \sum_{i=1}^{N_d} \frac{\beta^2 A^2}{\mu + \beta A g_i} \frac{(x-c)^2}{\sigma^4} g_i^2,$$

which varies as  $\beta$  as  $\beta \rightarrow \infty$ . On inverting the information matrix, the Cramér-Rao lower bound leads to a normalized deviation that varies as  $\beta^{-1/2}$ . Similarly, for the Gaussian width,

$$I_{44} = \sum_{i=1}^{N_d} \frac{\beta^2 A^2}{\mu + \beta A g_i} \frac{(x-c)^4}{\sigma^6} g_i^2$$

has the same behavior as  $I_{33}$  and so the normalized deviation varies as  $\beta^{-1/2}$  when  $\beta \rightarrow \infty$ . Increasing the number of counts in the Gaussian compared to a constant background, all three Gaussian variables improve equally fast for a large enough line-to-continuum ratio. As expected, the normalized deviation in the background gets worse with increasing  $\beta$  tending to  $\beta^{1/2}$  in the large  $\beta$  limit. The  $\beta$ -dependence in the parameter range shown is weak, since the leading term in the information matrix for the background ( $I_{11}$ ) contains no large  $1/g_i^2$  factors, unlike  $I_{22}$ ,  $I_{33}$ , and  $I_{44}$ .

### 3.6. Comparison of Line-Fitting Routines

The existence of a calculable limit to the precision an experiment can reach defines an independent standard against which line-fitting routines can be measured. Table 1 shows the results of such a comparison for six line-fitting routines available in the SolarSoft<sup>1</sup> library. A total of  $2^{20}$  spectra were fitted

<sup>1</sup> Available at <http://www.lmsal.com/solarsoft>.

TABLE 1  
DEPENDENCE ON FITTING ROUTINE

Routine	Initialization	$A$	$\lambda$	$\sigma$	$\mu$	Average $\chi^2$
CURVEFIT .....	True noise <sup>a</sup>	1.00	1.00	1.00	1.00	1.00
	Estimated noise <sup>b</sup>	1.00	1.00	1.01	1.02	1.01
CDS_GAUSS .....	True parameters <sup>c</sup>	1.07	1.25	1.45	1.20	1.07
	Estimated parameters <sup>d</sup>	1.07	1.25	1.45	1.19	1.07
MPCURVEFIT.....	True noise <sup>a</sup>	1.00	1.00	1.00	1.00	1.00
	Estimated noise <sup>b</sup>	1.00	1.01	1.01	1.02	1.01
GAUSSFIT.....	True parameters <sup>c</sup>	1.07	1.25	1.45	1.20	1.07
	Estimated parameters <sup>d</sup>	1.07	1.25	1.45	1.19	1.07
AMOEBa .....	True parameters <sup>c</sup>	1.31	1.91	2.57	13.0	2.43
	Estimated parameters <sup>d</sup>	1.78	2.26	6.93	21.1	3.56
POWELL .....	True parameters <sup>c</sup>	1.07	1.25	1.45	1.20	1.26

NOTE.—Dependence on fitting routine of average  $\chi^2$  and the variances in the fit parameters (normalized to the Cramér-Rao lower bound).

<sup>a</sup> The fit is weighted using the true emission profile.

<sup>b</sup> The spectrum to be fit is used as a weight.

<sup>c</sup> The true values of the emission profile parameters are used to seed the routine.

<sup>d</sup> The routine generates its own estimates of the emission-line parameters to seed the routine.

using each of the routines with the appropriate initialization (each spectrum was generated from the emission line of § 2.2 subject to Poisson statistics). Five of six routines have very similar performances, with the AMOEBA routine being noticeably worse than the others. The results show that the seeding of AMOEBA is critical to its performance; starting with a routine-generated initial guess is considerably worse than starting with the true parameters. This implies that if your initial guess is not close to the true values, then for each simulated emission line AMOEBA is much more likely to yield an answer more distant from the mean value than other routines. The other routines have broadly similar performances when compared to the Cramér-Rao limit. Note that there is a small, but present, effect on experimental precisions depending on whether these routines are seeded with either true noise/parameters compared to estimated noise/parameters. Initializing with estimated noise/parameters mimics a realistic situation faced by most users of these routines, and this study shows that experimental precision is not grossly affected by the use of good estimates.

### 3.7. Optimizing for Total Intensity

Observers are often interested in the total number of photons present in an emission line. This can be important for emission measure analysis, line diagnostics, and inversions to generate estimates of useful plasma parameters such as plasma temperature, density, and filling factor. The Cramér-Rao framework can be used to find under what conditions the measurement of integrated intensity is optimal.

Integrating across the line from  $-\infty$  to  $\infty$ , the total intensity is

$$I_T = \sqrt{2\pi}A\sigma, \quad (20)$$

where  $A$  and  $\sigma$  are the Gaussian amplitude and width, respectively. The actual number of photons measured is  $\gamma_T = \sum_{j=1}^{N_d} D_j$ . If  $\bar{A}$ ,  $\bar{c}$ , and  $\bar{\sigma}$  are estimates for a Gaussian emission line (amplitude, position, and width, respectively), then the estimated total intensity is  $\bar{I} = \bar{A} \sum_{j=1}^{N_d} \bar{g}_j$  for  $\bar{g}_j = \exp[-(x_j - \bar{c})^2 / (2\bar{\sigma}^2)]$ . If the line is well fitted and the estimated line width is a fraction of the spectral window width, then  $I_T$ ,  $\gamma_T$ , and  $\bar{I}$  are all approximately equal. If  $A$  is drawn from a distribution with

standard deviation  $\delta A$  and  $\sigma$  is drawn from a distribution with standard deviation  $\delta\sigma$ , then the standard deviation in  $I_T$ ,  $\delta I_T$ , is

$$\left(\frac{\delta I_T}{I_T}\right)^2 = \left(\frac{\delta A}{A}\right)^2 + \left(\frac{\delta\sigma}{\sigma}\right)^2. \quad (21)$$

An estimate of this quantity can be found by using the estimated Gaussian values and their estimated standard deviations.

Consider an experimental design that has a constant throughput of photons and is set up in such a way that the line width presented to the detector can be changed. If line width is small, only a few pixels are illuminated and the signal-to-noise ratio at those pixels is small. However, since only a few pixels are illuminated, the line width is not well determined. Conversely, when increasing the line width presented to the detector, the information about the line width gets better; however, the signal-to-noise ratio per pixel is correspondingly worse. Consequently, there should exist some intermediate line width that minimizes the standard deviation in the integrated intensity, making the measurement as precise as possible. Consider two lines that have the same integrated intensity; from equation (20),

$$A_2/A_1 = \sigma_1/\sigma_2. \quad (22)$$

If line 1 is fixed then this equation describes a relationship between the Gaussian amplitude and width for a line having the same integrated intensity. A Cramér-Rao lower bound calculation is performed on a set of emission lines that satisfy this relationship, generating values for  $(\delta A)^2$  and  $(\delta\sigma)^2$  that can be used to calculate a minimal value to  $(\delta I_T/I_T)^2$ . The Gaussian line 1 parameters are taken from the line parameters described in § 2.2. The Cramér-Rao lower bound calculation also includes a constant background; the calculation is repeated 3 times using a constant background emission 0.1, 1.0, and 10 times the value given for the emission line in § 2.2. The results are shown in Figure 6.

The Cramér-Rao lower bound calculation predicts optimal line widths minimizing the relative integrated intensity standard deviation for the observed line (for all three values to the background emission). The existence of minima is also confirmed by simulation. Changing the background value changes the behavior of  $(\delta I_T/I_T)^2$ , since information on the emission line depends on the entire system, including the background. When the background emission is fixed at the value given in § 2.2, it can be

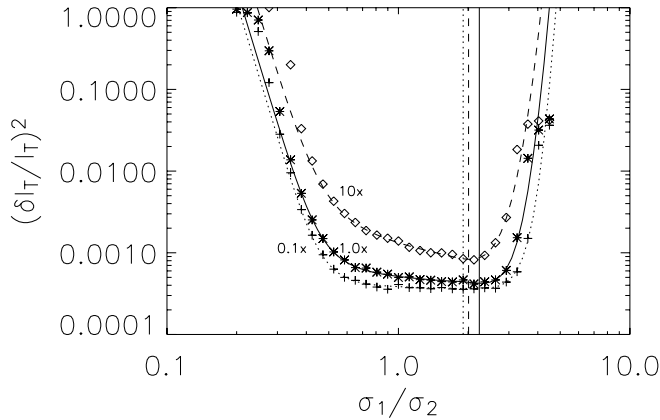


FIG. 6.—Square of the relative error in integrated intensity as a function of relative line width for three different values of constant background emission (0.1, 1, and 10 times the Fe background emission  $\mu$  in § 2.2, *dotted, solid, and dashed lines, respectively*, are the values predicted by the Cramér-Rao lower bound analysis). The original emission line (subscript 1) used is the Fe line in § 2.2; line 2 varies the line width and Gaussian amplitude so as to keep the integrated intensity constant for all values of  $\sigma_1/\sigma_2$ . The vertical lines indicate the positions of the minimum relative standard deviation. Also shown as plot symbols (Gaussian amplitude, *plus signs*; line position, *asterisks*; Gaussian width, *diamonds*; constant background, *triangles*) are the simulation-derived values of  $(\delta I_T/I_T)^2$  found by fitting 1024 Poisson-noisy emission profiles, calculating estimates of  $(\delta A)^2$  and  $(\delta\sigma)^2$  for insertion into eq. (21).

seen that the minimum of the  $(\delta I_T/I_T)^2$  is not at  $\sigma_1/\sigma_2 = 1$ , that is, the line width presented to our model detector is not optimized for measuring integrated intensity. Rather, the minimum occurs at  $\sigma_1/\sigma_2 = 2.26$ . The value of  $(\delta I_T/I_T)^2$  at  $\sigma_1/\sigma_2 = 1$  is  $\sim 1.2$  the value at the minimum. Therefore, changing the line width presented to the detector to  $\sigma_1/2.26$  would improve  $(\delta I_T/I_T)^2$  by 20%. The Cramér-Rao framework allows the experiment designer to explore different theoretical configurations; the question as to whether the extra effort required to optimize such an observation can be informed by studies such as those presented above but must be answered by the designer. Finally, it is interesting to note that the CDS-inspired Fe emission-line/detector model observations appear to exist in a portion of parameter space that is a reasonable compromise between knowledge of line amplitude, position, and width (see Fig. 1), and integrated intensity.

#### 4. CONCLUSION

The aim of this paper is to show that a Cramér-Rao framework is a convenient way to pose questions about the precision of spectrometer experiments and line fitting. The models chosen are relatively simple and are intended to be illustrative of the power and flexibility of this approach. The application of the Cramér-Rao lower bound to models of solar emission spectra shows that it is possible to characterize the precision capabilities of spectrometers in a variety of circumstances. The predictions are borne out by simulation in all the examples above.

In all the simulations described in § 3, CURVEFIT, a least-squares-based routine, was used to fit the simulated data. The variances calculated via simulation follow the Cramér-Rao lower bound very well, indicating that CURVEFIT is performing close to the limit for these problems. Why should this be? The Cramér-Rao lower bound arises from considering the maximum likelihood solution to equation (1), where the  $f_i$ 's are Poisson distributions for the emission-line statistics considered here (§ 2.2). However, since the mean values to these distribu-

tions are large, the Poisson distributions can be approximated by normal distributions of the form

$$\phi_i = \frac{1}{w_i\sqrt{2\pi}} \exp\left\{-\frac{[D_i - F_i(\mathbf{V})]^2}{2w_i^2}\right\}$$

for some  $w_i$  (either the true emission or the measured emission depending on the initialization of CURVEFIT). So,  $L \approx \prod_{i=1}^{N_d} \phi_i$  and  $\log L$  becomes a search for  $\tilde{\mathbf{V}}$  such that

$$\sum_{i=1}^{N_d} \frac{[D_i - F_i(\tilde{\mathbf{V}})]^2}{2w_i^2} + \sum_{i=1}^{N_d} \log(w_i\sqrt{2\pi})$$

is minimized. Since the right-hand term is constant with respect to the fit parameters, the expression above is a formulation of a weighted least-squares approach. Therefore, in the limit of large Poisson means and assuming a well-designed least-squares-based algorithm, the least-squares and maximum likelihood solutions approximate each other. Hence, condition (7) is approximately satisfied and so the least-squares algorithm performs close to the (Poisson based) Cramér-Rao limit.

There are a number of extensions that can be made to the basic models outlined here that will more accurately reflect a true spectrometric measurement. Real spectrometers have point-spread functions so that photons that should arrive at a given position on the detector actually appear on other, often neighboring pixels. This would have the effect of smearing out a Gaussian line and also changing the distribution function (or noise) at each detector pixel. The distribution function at each pixel would be the weighted sum of Poisson distributions, which, in general, is not a Poisson distribution (the overall probability distribution function [eq. (1)] would be a product of these weighted sums.) This effect should increase the Cramér-Rao lower bounds achievable. In addition, the noise distribution at each pixel is unlikely to just have purely Poissonian sources: other sources exist (pixel readout noise, for instance) and should also be taken into account when constructing Cramér-Rao models of spectrometers. For instance the noise response of CDS is known to be not purely Poissonian; as a first approximation, measurements in CDS appear to be drawn from Poisson distributions that have twice the mean one would expect. Clearly, this will influence achievable precisions.

The type of emission model will also influence achievable precisions. Many spectra have backgrounds that vary across the measured spectrum, breaking the symmetry of many of the results presented in this paper. Emission lines need not be Gaussian either. On 1998 June 25, the *SOHO* spacecraft was lost; on recovery and testing of CDS it was found that the emission profiles had changed significantly and are empirically described by  $B(\lambda) = A[(1-\alpha)G(\lambda) + \alpha W(\lambda)]$ , where  $G(\lambda) = \exp[(\lambda - C)^2/2\sigma^2]$ ,  $W(\lambda) = 1/\{1 + [(\lambda - C)/\sigma']^2\}$ , and  $\sigma' = 2\sigma(2 \ln 2)^{1/2}$ . The parameter  $\alpha$  is allowed to have different values on the red and blue sides of the line, introducing asymmetry to the line. This gives a total of five parameters, three for central Gaussian and one for each wing. Tests on post-recovery data (Thompson 1999, 2000) show that good fits are possible with asymmetric fits using the profile above. However, with more degrees of freedom noisy data can be fitted in many more ways and so it is expected that the precision with which the line parameters can be ascertained will worsen. Also, some spectra contain more than one emission line and often the two lines overlap, causing an apparent asymmetry in the line of interest (Taniguchi 1987; Smith & Shetrone 2000). Fitting both lines

increases the number of degrees of freedom of the fit and again we can expect precisions to worsen. These effects, which speak to more sophisticated and commonly occurring features of real spectrometers, will be studied in future papers.

The Cramér-Rao lower bound has shown itself to be useful in answering a variety of different questions about the knowledge achievable in spectrometric measurements. Further refinements in the description of model spectrometers that more accurately reflect the behavior of real spectrometers will lead to a better

understanding of the interplay of effects present in real spectrometric measurements.

This work is supported by NASA contract NNH04CC31C. The author wishes to thank N. H. Augustin, R. Fewster, and A. D. Gordon of the University of St. Andrews, Scotland, for their helpful discussions and suggestions. This paper is dedicated to the memory of Andrew Lidsey.

#### REFERENCES

- Barford, N. C. 1985, *Experimental Measurements: Precision, Error, and Truth* (2nd ed.; New York: Wiley)
- Cramér, H. 1946, *Mathematical Methods of Statistics* (Princeton: Princeton Univ. Press)
- Harrison, R. A., et al. 1995, *Sol. Phys.*, 162, 233
- Kendall, M. G., & Stuart, A. 1973, *The Advanced Theory of Statistics Vol. 2* (3rd ed.; London: Charles Griffin)
- Landman, D. A., Roussel-Dupré, R., & Tanigawa, G. 1982, *ApJ*, 261, 732
- Lenz, D. D., & Ayres, T. R. 1992, *PASP*, 104, 1104
- Rao, C. R. 1945, *Bull. Calcutta Math. Soc.*, 37, 81
- Smith, G. H., & Shetrone, M. D. 2000, *PASJ*, 112, 1320
- Taniguchi, Y. 1987, *ApJ*, 317, L57
- Thompson, W. T. 2000, *CDS Software Note 49* (ver. 5) (Chilton: CCLRC), [http://solar.bncs.rl.ac.uk/swnotes/cds\\_swnote\\_49.pdf](http://solar.bncs.rl.ac.uk/swnotes/cds_swnote_49.pdf)
- . 1999, *CDS Software Note 53* (ver. 1) (Chilton: CCLRC), [http://solar.bncs.rl.ac.uk/swnotes/cds\\_swnote\\_53.pdf](http://solar.bncs.rl.ac.uk/swnotes/cds_swnote_53.pdf)
- Winick, K. A. 1986, *J. Opt. Soc. Am. A*, 3, 1809